Available online at www.sciencedirect.com
ScienceDirect
Journal of Power Sources 162 (2006) 636–643
JOURNAL OF POWER SOURCES
www.elsevier.com/locate/jpowsour

Synthesis and physicochemical properties of $LiAl_{0.05}Mn_{1.95}O_4$ cathode material by the ultrasonic-assisted sol–gel method

Tingfeng Yi *, Xinguo Hu, Kun Gao

Department of Applied Chemistry of Harbin Institute of Technology, Harbin 150001, PR China

Received 13 May 2006; received in revised form 30 June 2006; accepted 9 July 2006
Available online 14 August 2006

Abstract

Spinel $LiAl_{0.05}Mn_{1.95}O_4$ has been successfully synthesized by a new ultrasonic-assisted sol–gel (UASG) method. The structure and physicochemical properties of this as-prepared powder compared with the pristine $LiMn_2O_4$ and $LiAl_{0.05}Mn_{1.95}O_4$ synthesized by the traditional sol–gel method were investigated by differential thermal analysis (DTA) and thermogravimetery (TG), powder X-ray diffraction (XRD), X-ray photoelectron spectroscopy (XPS), Fourier transform infrared (FT-IR) spectroscopy, scanning electron microscopy (SEM), cyclic voltammetry (CV), and galvanostatic charge–discharge testing in detail. The results show that all samples have high phase purity, and ultrasonic process plays an important role in controlling morphology; $LiAl_{0.05}Mn_{1.95}O_4$ has higher Mn oxidation state, and the absorption peak of Mn(III)─O and Mn(IV)─O bonds has blue shift because of the doped Al. CV confirms that the $LiAl_{0.05}Mn_{1.95}O_4$ sample (UASG) has a good reversibility and its structure is very advantageous for the transportation of lithium ions. The charge–discharge tests indicate that $LiAl_{0.05}Mn_{1.95}O_4$ (UASG) has nearly equal initial capacity with $LiMn_2O_4$ (sol–gel) at 1*C* discharge rate, but $LiAl_{0.05}Mn_{1.95}O_4$ (UASG) has higher discharge potential than that of $LiMn_2O_4$ (sol–gel). In addition, $LiAl_{0.05}Mn_{1.95}O_4$ (UASG) has higher discharge potential and capacity than that of $LiAl_{0.05}Mn_{1.95}O_4$ (sol–gel) at 1*C* discharge rate, and $LiAl_{0.05}Mn_{1.95}O_4$ (UASG) has high capacity retention at *C*/3 and 1*C* discharge rate among three samples after 50 cycles, which reveals that the sample obtained via UASG method, has the best electrochemical performance among three samples.

Keywords: Lithium ion battery; Spinel $LiAl_{0.05}Mn_{1.95}O_4$; Ultrasonic-assisted sol–gel method; Synthesis; Physicochemical properties

1. Introduction

Spinel $LiMn_2O_4$ has received a great deal of attention as the most promising cathode material for lithium ion batteries because of its low cost and lower toxicity compared with the layered oxides $LiCoO_2$ and $LiNiO_2$ [1,2]. In spite of these advantages, $LiMn_2O_4$ has the problem of severe capacity fading during charge–discharge cycles, which makes it unsuitable for commercial performances. This problem has been discussed based on the following factors: manganese dissolution [3], electrolyte decomposition at high potentials [4], Jahn–Teller distortion at the deeply discharged state [5], and lattice instability [6]. Of the above factors, dissolution of manganese into the electrolyte during cycling is believed to be the main one. To solve these problems, many researchers have studied the mechanism of capacity fading and have put forward some method to overcome capacity fading by doping the spinel with several cations, such as Al [7–9], transition metal ions [10–14], etc. to enhance the structural stability. It is well known that the aluminum is abundant, less expensive, and lighter than the transition metal group, so Al-substituted Li–Mn–O spinel is expected to be a cathode material with lower cost than transition metals substituted $LiMn_2O_4$. Moreover, many researchers [7–9] have reported the Al-substituted $LiAl_xMn_{2-x}O_4$ spinel showed relatively good electrochemical performances.

The charge–discharge capacity and cycle performance of $LiMn_2O_4$ were greatly affected by synthesis methods and condition [15]. In general, $LiAl_{0.05}Mn_{1.95}O_4$ was prepared by a conventional solid-state method. However, it requires prolonged heat treatment at relatively high temperatures with repeatedly intermediate grinding. Moreover, this method does not provide good control on the crystalline growth, compositional homogeneity, morphology and microstructure. The sol–gel method gives $LiMn_2O_4$ with a fine particle size, a narrow size

* Corresponding author. Tel.: +86 451 8641 3751; fax: +86 451 8622 1048.
E-mail address: tfyihit@hit.edu.cn (T. F. Yi).

0378-7753/$ – see front matter © 2006 Elsevier B.V. All rights reserved.
doi:10.1016/j.jpowsour.2006.07.019

distribution, and uniform composition, which leads to high electrochemical performance, so it has been widely used to prepare positive electrode materials of lithium ion batteries [2].

In present work, Al-doped $LiAl_{0.05}Mn_{1.95}O_4$ powders were successfully prepared by a new simple ultrasonic-assisted sol–gel (UASG) method. The structure, morphology and electrochemical properties of the products have been investigated in detail.

2. Experimental

2.1. Materials preparation

The samples of spinel $LiAl_{0.05}Mn_{1.95}O_4$ were prepared by the ultrasonic-assisted sol–gel method using adipic acid as a chelating agent. Stoichiometric amounts of reactants $Li(CH_3COO)\cdot 2H_2O$(AR, 99%), $Al(NO_3)_3\cdot 9H_2O$(AR, 99%) and $Mn(CH_3COO)_2\cdot 6H_2O$(AR, 99%) were dissolved in distilled water to give a solution with mild stirring. An aqueous solution of adipic acid was then added at 1:1 molar ratios with the total metal ions. The pH of the mixed solution was maintained 6.5 by adding ammonium hydroxide solution. Thereafter, the mixed solution was constantly shocked at about 80 °C for about 10 h in a KQ-100 VDE numerical-control ultrasonic cleaner (Kunshan ultrasonic instrument Co. Ltd., China) to remove excess water until a gel was obtained. The experiments were carried out in a batch reactor of volume up to 4 L. The ultrasonic apparatus consisted of a generator, a converter and a sonotrode. The frequency and power are set at 28 kHz and 50 W, respectively. Then, the gel was dried in vacuum drying oven for 12 h at 110 °C, resulting in the formation of amorphous powders. The resulting amorphous powder was decomposed at 400 °C for 5 h in air to remove the organic contents. Then, the resulting precursor was ground to fine powders and calcined at 800 °C in air for 10 h to obtain the final spinel product.

2.2. Materials characterization

Differential thermal analysis (DTA) and thermogravimetery (TG) measurements were performed in air from room temperature to 900 °C with a ZRY-2P thermal analysis system (Shanghai, China) under a scanning rate of 5 °C min^{-1}. Powder X-ray diffraction (XRD) was performed on Rigaku D/MAX-RC X-ray diffractometer with Cu $K\alpha_1$ (45 kV, 50 mA, step size = 0.02°, $10° < 2\theta < 80°$) monochromated radiation in order to identify the crystalline phase of the materials. X-ray photoelectron spectroscopy (XPS) was collected to study the Mn oxidation state of materials. All the XPS spectra were performed on American PHI5700 ESCA with a non-monochromatic Mg Kα (1253.6 eV) light source. The C 1s XPS at 284.62 eV was used as the calibration of the spectra. Fourier transform infrared (FT-IR) spectroscopy of the samples was performed using a Nicolet Nexus 360 FTIR spectrophotometer. A total of 1.5 mg sample dried at 120 °C was thoroughly mixed with 200 mg KBr and pressed into pellets and the scans were performed immediately to avoid water absorption. The frequency range was 800–350 cm^{-1}.The particle morphologies of the samples were examined with a scanning electron microscope (SEM, Hitachi, S-570). Cyclic voltammetry (CV) was measured on an electrochemical workstation (CHI 630A) at a scan rate of 0.1 mV s^{-1} between 3.3 V and 4.5 V (versus Li/Li^+). Charge–discharge performance of the cell was characterized galvanostatically on BTS 5 V/5 mA battery testing system (Shenzhen, China) at *C*/3 charge rate and *C*/3 and 1*C* discharge rate between 3.3 V and 4.5 V (versus Li/Li^+), respectively.

2.3. Preparation of lithium ion batteries

For the preparation of cathode sheets, a slurry was formed by mixing the active material (85%), acetylene black (10%) and binder (5 wt% polyvinylidene fluoride, PVDF, dissolved in *N*-methyl-2-pyrrolidone, NMP). The slurry was coated onto an aluminum current collector. The electrodes were dried under vacuum at 120 °C overnight and then punched and weighed. The batteries were assembled in a glove box under a dry and high purity argon atmosphere (99.999%). The complete coin cell comprises a cathode, a celgard 2300 (polypropylene) as the separator and a lithium foil anode. One molar of $LiPF_6$ (battery grade) dissolved in a mixture of ethylene carbonate (EC, battery grade) and dimethyl carbonate (DMC, battery grade) (1:1 by volume) was used as the electrolyte.

3. Results and discussion

3.1. TG-DTA analysis

Fig. 1 shows the TG and DTA curves of the precursor with $LiAl_{0.05}Mn_{1.95}O_4$ synthesized by UASG method.

There are four temperature intervals where significant mass loss can be detected. The first one is the interval between room temperature and 170 °C that corresponds to the superficial water loss due to the hygroscopic nature of the precursor complex. The second one is in the range between 170 °C and 300 °C that corresponds to the loss of water of chemical bond water in the sample. In the third region 300–360 °C, the exothermic peak observed at 355.7 °C is accompanied by noticeable weight lose in the TG curve. It can be considered as a result of the decomposition of

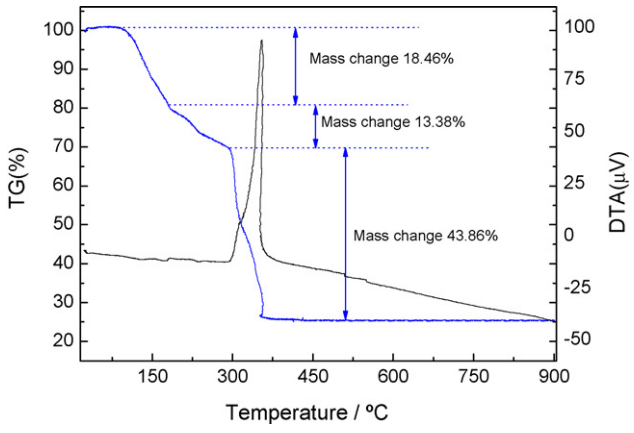

Fig. 1. TG–DTA curves for the thermal decomposition of the precursor $LiAl_{0.05}Mn_{1.95}O_4$ synthesized by UASG method.

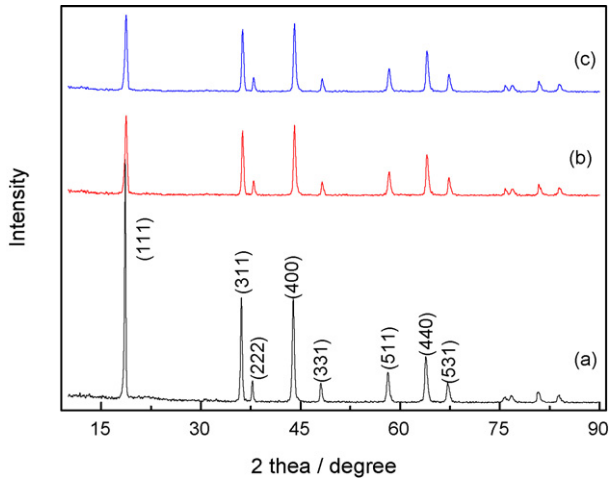

Fig. 2. X-ray powder diffraction patterns obtained from the prepared samples: (a) $LiMn_2O_4$ obtained from sol–gel method; (b) $LiAl_{0.05}Mn_{1.95}O_4$ obtained from sol–gel method; (c) $LiAl_{0.05}Mn_{1.95}O_4$ obtained from UASG method.

the inorganic and the organic constituents of the precursor followed by crystallization of spinel $LiAl_{0.05}Mn_{1.95}O_4$ phase. In the last region, the TG curve becomes flat and no sharp peaks can be observed in the DTA curve, indicating that no phase transformation occurs, and that any further heating only makes the structure of samples more crystalline.

3.2. Structure characterization of materials

Typical powder X-ray diffraction patterns of $LiMn_2O_4$ and $LiAl_{0.05}Mn_{1.95}O_4$ samples synthesized by different methods are given in Fig. 2.

The diffraction patterns of three samples were similar, with all the peaks indexable in the *Fd3m* space group with a cubic lattice. It is well-known that the position and the FWHM of the (4 0 0) peak are important factors indicating the degree of crystallinity in $LiMn_2O_4$ spinel powder. The structure parameters of $LiMn_2O_4$ and $LiAl_{0.05}Mn_{1.95}O_4$ powders are listed in Table 1.

The intensity of the (4 0 0) peak for $LiMn_{1.95}Al_{0.05}O_4$ samples obtained from UASG and sol–gel method are lower than that of $LiMn_2O_4$ powders due to the small X-ray scattering factor of Al, though they are smaller FWHM value of the (4 0 0) peak than that of $LiMn_2O_4$ powders, and the positions of diffraction peaks are progressively shifted toward a higher angel, meaning that lattice parameter decrease as shown in Table 1, so Al-substituted $LiMn_2O_4$ compositions exhibit better crystallinity than the pure $LiMn_2O_4$. It may be explained by the facts that: (1) Al^{3+} ion (0.053 nm) has smaller ionic radius than that of Mn^{4+}(0.060 nm) and Mn^{3+}(0.066 nm) [16]; (2) the dopant of Al^{3+} ion results in the formation of more Mn^{4+} cation, and the atomic radius of Mn^{4+} is smaller than that of Mn^{3+}; (3) the bond energy of the Al–O (512 kJ mol^{-1}) is much greater than that of Mn–O (402 kJ mol^{-1}), so it has a higher octahedral site preference energies (OPE) which results in diminution of the bond length. The aforementioned features of the Al-substituted $LiMn_2O_4$ compositions are very desirable for being employed as the electrode material to improve the electrochemical properties of spinel $LiMn_2O_4$ cathode materials for lithium rechargeable batteries. Moreover, some works have shown that the intensity ratio of the two peaks, I(3 1 1)/I(4 0 0), is closely related to the electrochemical properties of spinel lithium manganese oxide. For example, it has been reported that Al-doped Li–Mn–O spinel compounds with the I(3 1 1)/I(4 0 0) ratios between 0.96 and 1.1 have shown better electrochemical properties than those outside this region [7]. In this study, the I(3 1 1)/I(4 0 0) ratio value of $LiMn_{1.95}Al_{0.05}O_4$ samples only obtained from UASG method exists in this region. Comparing the I(3 1 1)/I(4 0 0) ratios of spinel lithium manganese oxides obtained by different methods and those of Al-doped Li–Mn–O spinel, it is expected the $LiMn_{1.95}Al_{0.05}O_4$ samples obtained from UASG to show better electrochemical performance than other samples. The narrowest (4 0 0) peak of the sample $LiAl_{0.05}Mn_{1.95}O_4$ obtained from the UASG method also indicate that the crystallinity of the compound by this new simple method is better than that of the sample by the sol–gel method.

X-ray photoelectron spectroscopy has been widely used to study the electronic structure of materials. The XPS binding energies provide useful information on the oxidation states of different elements in materials. The Mn 2p XPS spectrum of $LiMn_2O_4$ and $LiAl_{0.05}Mn_{1.95}O_4$ are plotted in Fig. 3.

It is shown in Fig. 3 that the Mn $2p_{3/2}$ binding energy is found to be 642.78 eV and 642.63 eV for the prepared samples $LiAl_{0.05}Mn_{1.95}O_4$ and $LiMn_2O_4$, respectively. Shaju et al. have reported that the Mn $2p_{3/2}$ binding energies of $Mn^{3+}$and Mn^{4+} are at 641.9 eV and 643.2 eV, respectively [17]. In this study, the Mn $2p_{3/2}$ binding energies were in this region, indicating that the Mn oxidation state in spinel $LiAl_{0.05}Mn_{1.95}O_4$ and $LiMn_2O_4$ was between +3 and +4, and $LiAl_{0.05}Mn_{1.95}O_4$ had higher Mn oxidation state because of the doped Al. The increasing of the Mn oxidation state leads to the shrinkage of the spinel framework because the ionic radius of Mn^{4+} is smaller than that of Mn^{3+}, resulting in smaller lattice constants. The volume change during the cycling process may be suppressed by this way.

Table 1
Structure parameters of $LiMn_2O_4$ and $LiAl_{0.05}Mn_{1.95}O_4$ samples

Samples	Lattice parameter (Å)[a]	Unit cell volume (Å^3)	I(3 1 1)/I(4 0 0)	FWHM of the (4 0 0) peak
$LiMn_2O_4$ (sol–gel)	8.238	559.07	0.94	0.300
$LiAl_{0.05}Mn_{1.95}O_4$ (sol–gel)	8.211	552.98	0.92	0.229
$LiAl_{0.05}Mn_{1.95}O_4$ (UASG)	8.209	551.77	0.96	0.225

[a] Calculated through the least square program method from the diffraction data.

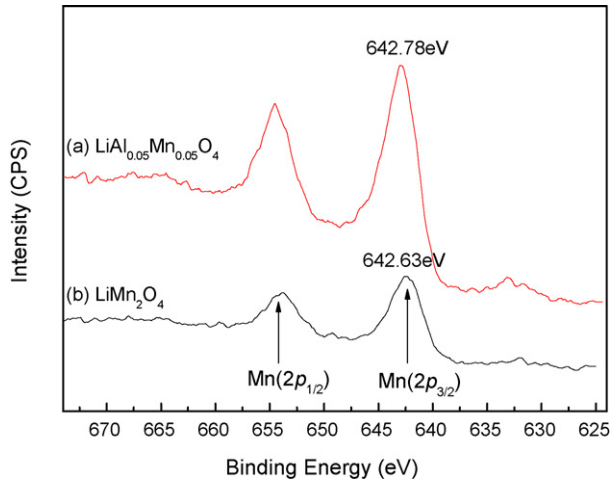

Fig. 3. Mn 2p XPS spectrum of the prepared samples: (a) $LiAl_{0.05}Mn_{1.95}O_4$ obtained from UASG method and (b) $LiMn_2O_4$ obtained from sol–gel method.

Vibrational modes attributed to the motion of cations with respect to their oxygen neighbors are sensitive to the point group symmetry of the cations in the oxygen host matrix [18]. Hence, the local environment of the cations in a lattice of close-packed oxygen can be studied by FT-IR spectroscopy. For the Al-doped Li–Mn–O spinel, infrared spectra (IR) shows that the replacement of manganese with aluminum at the octahedral 16d sites affects the vibration mode of Mn–O bond, as shown in Fig. 4.

It's found that the FTIR absorption of the $LiAl_{0.05}Mn_{1.95}O_4$ and $LiMn_2O_4$ samples between 612 cm^{-1} and 617 cm^{-1} and between 511 cm^{-1} and 513 cm^{-1} are attributed to the asymmetric stretching modes of the MnO_6 group, based on the results of recent studies [19]. It has been reported that the Li–O stretching bands at 536 cm^{-1} has been observed in layered $LiCoO_2$ [20]. However, the Li–O vibration of the both spinels can not be recognized in this range (see Fig. 4). It has been reported that the width and the intensity of the vibrational bands of alkali metal cations (Li^+) are dependent on the cation mass in some cases [21], and the vibrational modes of transition metal oxide spinels

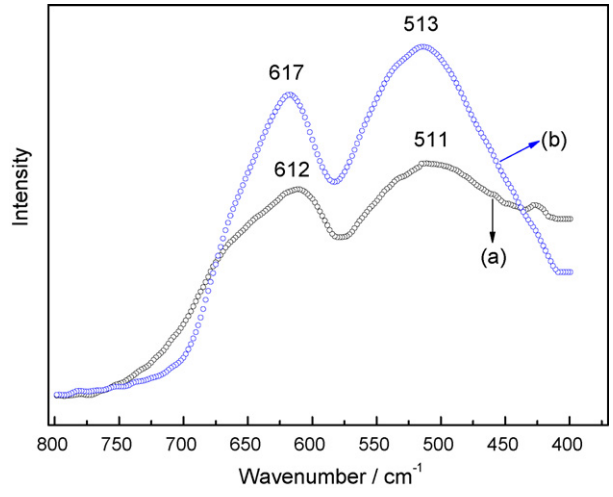

Fig. 4. FTIR absorption spectra of the prepared samples: (a) $LiMn_2O_4$ obtained from sol–gel method and (b) $LiAl_{0.05}Mn_{1.95}O_4$ obtained from UASG method.

are attributed to all the atoms in the framework [22], so the Li–O and Mn–O vibration may be overlaped.

In contrast, the Mn–O stretching bands at 612 cm^{-1} and 511 cm^{-1} have blue shift to 617 cm^{-1} and 513 cm^{-1}, respectively, which may be related to the atomic mass of aluminum and the strength of M–O bond. In the Al-doped spinels, the Al^{3+} will occupy the octahedral 16d sites to replace the Mn^{3+}. The stretching vibration frequency of Mn(III)–O bond of MnO_6 octahedron increases because the atomic mass of aluminum ion is less than that of manganese ion, so the absorption peak at 511 cm^{-1} has a blue shift. In addition, because of the shrinkage of unit cell volume of $LiAl_{0.05}Mn_{1.95}O_4$, the stretching vibration frequency of Mn(IV)–O bond increase, so the absorption peak at 612 cm^{-1} also has a blue shift.

It is well known that the surface morphology and particle size distribution are also important factors for electrochemical performance of the lithium secondary batteries, so particle size and morphology of all samples have been examined by scanning electron microscopy. Fig. 5 exhibits scanning electron micrographs (SEM) of spinel samples obtained from different synthesis methods.

All of the prepared powders have the uniform, nearly cubic structure morphology with narrow size distribution which is less than 1 μm. However, there is greater extent of agglomeration of particles in the $LiMn_2O_4$ samples. The $LiAl_{0.05}Mn_{1.95}O_4$ samples obtained from sol–gel method have bigger particle size than that of $LiAl_{0.05}Mn_{1.95}O_4$ samples obtained from UASG method. The results indicate that the ultrasonic process can make the solid powders dispersed more uniformly in the liquid substances and to some extent effectively restrain the agglomeration of solid powders. Furthermore, both $LiAl_{0.05}Mn_{1.95}O_4$ samples have octahedral morphology with well ordered direction, which suggests that Al ions were successively substituted for Mn in $LiAl_{0.05}Mn_{1.95}O_4$ host structure. In addition, it has been reported that spinel lithium manganese oxide of octahedral morphology improves the thermal stability [23]. The aforementioned features of $LiAl_{0.05}Mn_{1.95}O_4$ samples obtained from UASG method are very desirable for being employed as the electrode material to improve the electrochemical properties of spinel lithium manganese oxide cathode materials for lithium rechargeable batteries.

3.3. Electrochemical performance

The cyclic voltammogram properties of $LiAl_{0.05}Mn_{1.95}O_4$ samples obtained from different synthesis methods were tested. Cyclic voltammograms (sweep rate: 0.1 mV s^{-1}) in the potential region of 3.3–4.5 V are presented in Fig. 6, and their values of the CV peak are listed in Table 2.

It can be seen from Fig. 6 that $LiAl_{0.05}Mn_{1.95}O_4$ samples obtained from sol–gel method are two pairs of redox current peaks at about 3.85 V/4.12 V and 3.99 V/4.27 V, and $LiAl_{0.05}Mn_{1.95}O_4$ samples obtained from UASG method are two pairs of redox current peaks at about 3.96 V/4.06 V and 4.09 V/4.17 V, on each cyclic voltammogram. These two pairs of redox peaks correspond to a two-step reversible intercalation reaction, in which lithium ions occupy two different tetragonal

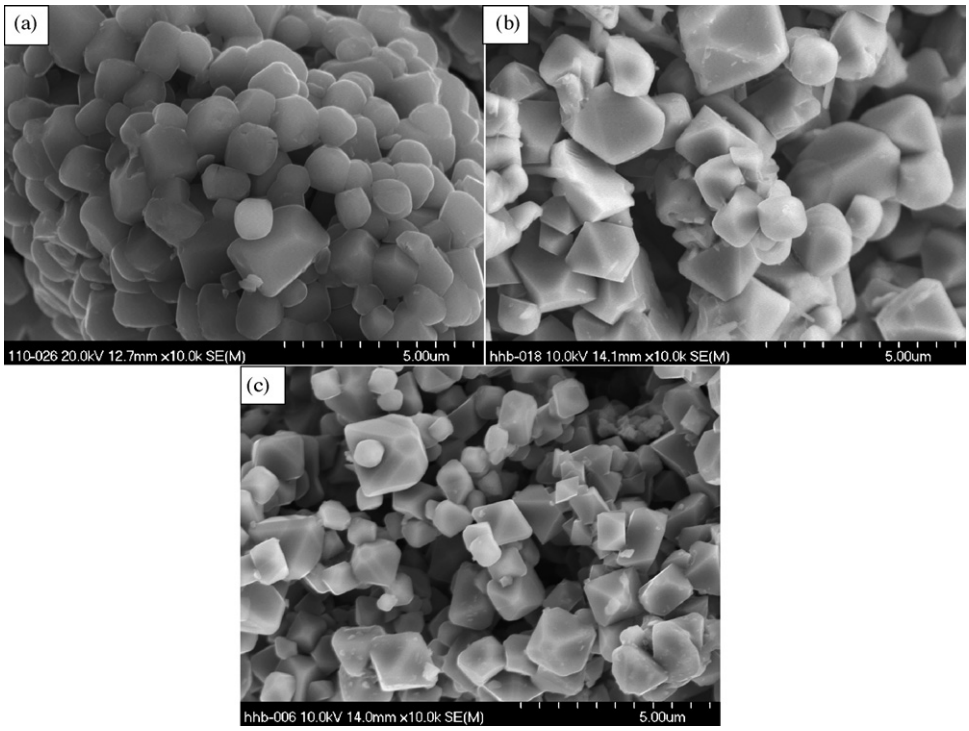

Fig. 5. Scanning electron micrographs (SEM) of (a) $LiMn_2O_4$ obtained from sol–gel method; (b) $LiAl_{0.05}Mn_{1.95}O_4$ obtained from sol–gel method; (c) $LiAl_{0.05}Mn_{1.95}O_4$ obtained from UASG method.

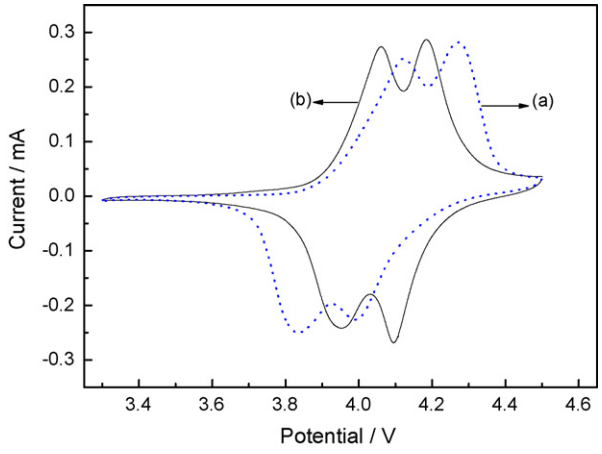

Fig. 6. Cyclic voltammetry for spinel $LiAl_{0.05}Mn_{1.95}O_4$: (a) synthesis by sol–gel method and (b) synthesis by UASG method at sweep rate 0.1 mV s^{-1}.

8a sites in spinel $Li_xMn_2O_4$ ($x<1$). However, during the oxidation procedure, it is found that the $LiAl_{0.05}Mn_{1.95}O_4$ sample obtained from sol–gel method has higher oxidation potential than that of $LiAl_{0.05}Mn_{1.95}O_4$ sample obtained from UASG method corresponding to the extraction of Li^+ ions. Deintercalation of Li^+ ions at higher potential indicates that more driving force is necessary to impel the lithium ions from the host structure to the anode [24]. This implies that the $LiAl_{0.05}Mn_{1.95}O_4$ sample obtained from UASG method has better reversibility.

In addition, the redox peaks of both $LiAl_{0.05}Mn_{1.95}O_4$ electrodes are sharp and show well-defined splitting, which indicates that the powders exhibit good crystallinity. For $LiAl_{0.05}Mn_{1.95}O_4$ samples obtained from UASG method, the measured value of the ratio for peak currents I_{pc}/I_{pa} and the separation of peak potentials $\Delta\varphi_p$ are nearly 1 and 80 mV, respectively; however, for $LiAl_{0.05}Mn_{1.95}O_4$ samples obtained from sol–gel method, the value of I_{pc}/I_{pa} and $\Delta\varphi_p$ are 1.21 and 280 mV as given in Table 2, respectively, which demonstrates that lithium ions are intercalation and deintercalation reversible in the $LiAl_{0.05}Mn_{1.95}O_4$ compounds from UASG method and this redox system remains in equilibrium throughout the potential scan [25]. This also confirms that the $LiAl_{0.05}Mn_{1.95}O_4$ sample obtained from UASG method has a good reversibility and its structure is very advantageous for the transportation of lithium ions.

The charge–discharge curves of all electrode materials at *C*/3 charge–discharge rate between 3.3 V and 4.5 V are shown

Table 2
Values of the CV peaks for $LiAl_{0.05}Mn_{1.95}O_4$ sample synthesized by different methods

Samples	φ_{pa} (V)	φ_{pc} (V)	$\Delta\varphi_p$ (mV)[a]	I_{pa} (mA)	I_{pc} (mA)	I_{pc}/I_{pa}
$LiAl_{0.05}Mn_{1.95}O_4$ (sol–gel)	3.99	4.27	280	0.23	0.28	1.21
$LiAl_{0.05}Mn_{1.95}O_4$ (UASG)	4.09	4.17	80	0.27	0.29	1.07

[a] $\Delta\varphi_p = \varphi_{pa} - \varphi_{pc}$.

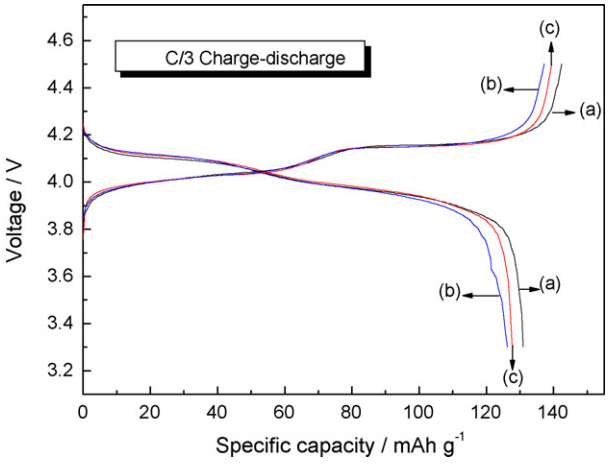

Fig. 7. Voltage (V)-specific capacity (mAh g^{-1}) profiles obtained from (a) $LiMn_2O_4$ obtained from sol–gel method; (b) $LiAl_{0.05}Mn_{1.95}O_4$ obtained from sol–gel method; (c) $LiAl_{0.05}Mn_{1.95}O_4$ obtained from UASG method during charge–discharge step in the 3.3–4.5 V region at *C*/3.

in Fig. 7. The discharge curves of all electrode materials at 1*C* discharge rate between 3.3 V and 4.5 V are given in Fig. 8.

All charge–discharge curves exhibit two obvious discharge plateaus associated with two-stage mechanism of the electrochemical lithium intercalation at 4.0–4.1 V and 3.9–4.0 V. The first voltage plateau at about 4.0 V is attributed to the removal of lithium ions from half of the tetrahedral sites in which Li–Li interactions occur. The second voltage plateau observed at about 4.1 V is due to the removal of lithium ions from the other tetrahedral sites in which lithium ions do not have Li–Li interactions. The initial capacities of $LiMn_2O_4$ (sol–gel), $LiAl_{0.05}Mn_{1.95}O_4$ (sol–gel), and $LiAl_{0.05}Mn_{1.95}O_4$ (UASG) are 130.9 mAh g^{-1}, 126.2 mAh g^{-1} and 127.9 mAh g^{-1}, respectively. $LiMn_2O_4$ has the highest discharge capacity among three samples, which is due to the highest amount of Mn^{3+} ions in $LiMn_2O_4$ spinel phase. During charge–discharge, the change of manganese valence

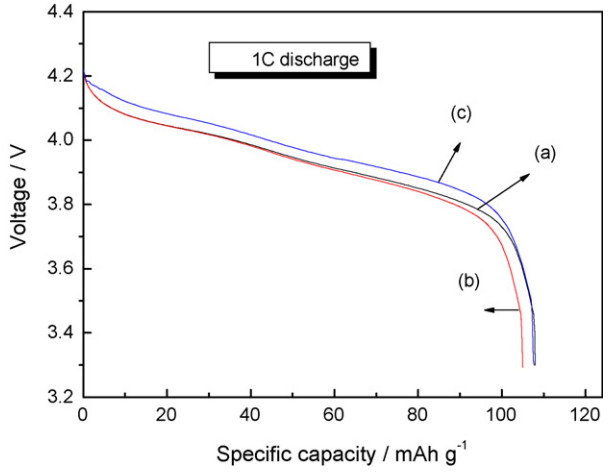

Fig. 8. Voltage (V)-specific capacity (mAh g^{-1}) profiles obtained from (a) $LiMn_2O_4$ obtained from sol–gel method; (b) $LiAl_{0.05}Mn_{1.95}O_4$ obtained from sol–gel method; (c) $LiAl_{0.05}Mn_{1.95}O_4$ obtained from UASG method during discharge step in the 3.3–4.5 V region at 1*C*.

state occurs as follows:

$$LiMn_2O_4 \Leftrightarrow Li_{1-x}Mn_2O_4 + xLi + xe^-$$

The reaction shows that during the charge, the deintercalation of lithium ion from the spinel is accompanied by an oxidation of Mn^{3+} to Mn^{4+}. So the more Mn^{3+} that exists in $LiMn_2O_4$, the more lithium ion can deintercalate from the host, so more lithium ion can intercalate into the anode, and increase the discharge capacity.

The initial capacities of $LiMn_2O_4$ (sol–gel), $LiAl_{0.05}Mn_{1.95}O_4$ (sol–gel), and $LiAl_{0.05}Mn_{1.95}O_4$ (UASG) at 1*C* discharge rate are 108.0 mAh g^{-1}, 105.0 mAh g^{-1} and 107.7 mAh g^{-1}, respectively. It is clearly to see that $LiAl_{0.05}Mn_{1.95}O_4$ (UASG) has nearly equal initial capacity with $LiMn_2O_4$ (sol–gel) at high discharge rate, but $LiAl_{0.05}Mn_{1.95}O_4$ (UASG) has higher discharge potential than that of $LiMn_2O_4$ (sol–gel). In addition, $LiAl_{0.05}Mn_{1.95}O_4$ (UASG) has higher discharge potential and capacity than that of $LiAl_{0.05}Mn_{1.95}O_4$ (sol–gel), which reveals that the sample obtained via UASG method has the best electrochemical performance among three samples. With increasing the discharge rate, the discharge capacity descend quickly, and the discharge potential and discharge plateaus also change a lot, which two discharge voltage plateaus of 4 V become one plateaus.

In order to study the influence of doping Al^{3+} ions and synthesis method on the cycle ability of spinel lithium manganese oxide, the result of the cycle profile of Al-doped spinel is illustrated in Fig. 9. Table 3 summarizes the cycling performance of the prepared powders discharged at different current densities from Fig. 9.

It is found that both $LiAl_{0.05}Mn_{1.95}O_4$ samples have better cycle ability as given in Fig. 9, which is believed to be related with the doped aluminum. This may be explained that the Jahn–Teller distortion is effectively restrained because Al^{3+} ions substituted Mn^{3+} ions. Compared with the $LiAl_{0.05}Mn_{1.95}O_4$ synthesized by sol–gel method, the Al-doped $LiAl_{0.05}Mn_{1.95}O_4$ obtained from the new simple UASG method has a larger initial discharge capacity and much higher capacity retention rate after 50 cycles as shown in Table 3, which is due to be related with its better crystallinity and regular morphology, also this comment is well consistent with the SEM results mentioned above.

$LiAl_{0.05}Mn_{1.95}O_4$ (UASG) exhibits the best capacity retention upon cycling and high current discharge performance among all samples. The excellent recharge ability for the Al-doped spinels results from a homogeneous insertion/extraction reaction proceeding over the entire intercalation region. Accordingly, it is obvious that the UASG method is more suitable to prepare the spinel $LiMn_2O_4$ with a good cubic spinel structure and cycle performance. This new method appears to be a better alternative to the traditional sol–gel method for synthesizing lithium ion battery cathode materials. As we know, the high rate discharge capability is one of the most important electrochemical performances in the application of electrode and battery, and the excellent rate capability of the $LiAl_{0.05}Mn_{1.95}O_4$ (UASG) makes it attractive particularly for a practical application because of the ultrasonic-catalysis during the preparation of gel precursor, which the ultrasonic process can make the solid

Table 3
Cycle performance datum of the prepared powders at different discharge rate for the 1st cycle and the 50th cycle

Samples	Discharge rate	Initial discharge capacity (mAh g^{-1})	Discharge capacity after 50 cycles (mAh g^{-1})	Capacity retention ratio (%)[a]
$LiMn_2O_4$ (sol–gel)	*C*/3	130.9	113.7	86.86
	1*C*	108.0	85.56	79.22
$LiAl_{0.05}Mn_{1.95}O_4$ (sol–gel)	*C*/3	126.2	115.7	91.68
	1*C*	105.0	87.63	83.46
$LiAl_{0.05}Mn_{1.95}O_4$ (UASG)	*C*/3	127.9	120.6	94.29
	1*C*	107.7	93.24	86.57

[a] The capacity retention ratio is according to the equation: $(C_{50}/C_1) \times 100\%$, where C_{50} is the discharge capacity after 50 cycles and C_1 is the initial discharge capacity.

powders dispersed more uniformly in the liquid substances. The mechanism of ultrasonic-catalysis is not related with the direct interaction between sound waves and molecules, but the liquid vacuum process. When air bubbles collapse, the local temperature will be above 5000 K and the local pressure will be up to 5×10^7 Pa. Meanwhile, the change rate of temperature is about 109 K s^{-1} and there are intense bow wave and 400 km h^{-1} current, which offers a very special physical condition [26,27]. Under such a condition, ultrasonic wave treating can increase the uniformity of the aipic acid molecules and metal ions arrangement. Due to the strong stirring of ultrasonic wave, the diffusion and the transfer of metal ions become easier, and the precursors can form a homogeneous single phase of precise stoichiometry. Therefore, ultrasonic wave treating can significantly increase physicochemical properties, and this comment is well consistent with the experimental results mentioned above in this paper.

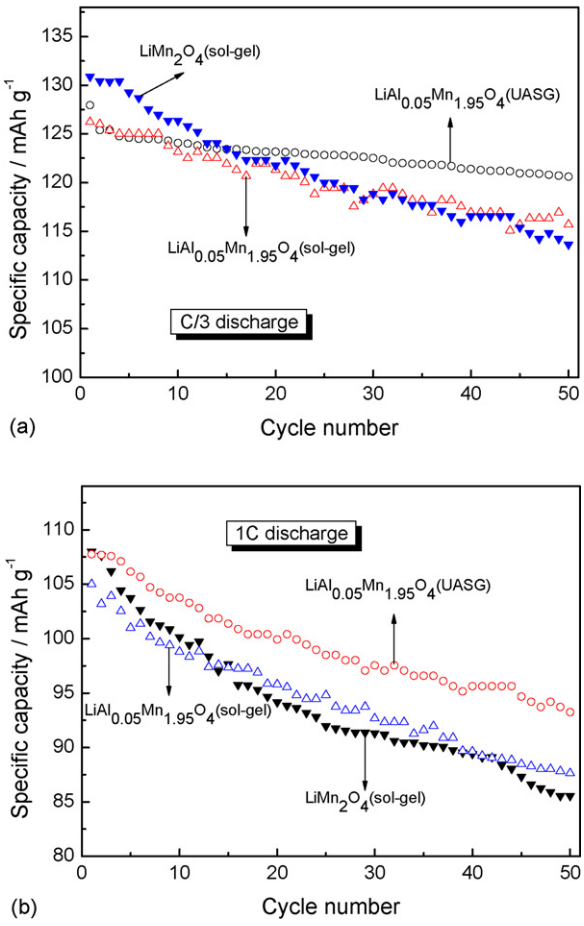

Fig. 9. Capacity vs. cycle number for $LiMn_2O_4$ (sol–gel), $LiAl_{0.05}Mn_{1.95}O_4$ (sol–gel), and $LiAl_{0.05}Mn_{1.95}O_4$ (UASG) cells at a discharge current density of (a) *C*/3 and (b) 1*C* between 3.3 V and 4.5 V.

4. Conclusions

In this paper, aluminum doped spinel $LiAl_{0.05}Mn_{1.95}O_4$ with spinel structure and excellent electrochemical performance have been successfully prepared by a new UASG method. $LiAl_{0.05}Mn_{1.95}O_4$ (UASG) indicates that the crystallinity of the compound by this new simple method is better than that of the sample by the sol–gel method. $LiAl_{0.05}Mn_{1.95}O_4$ has higher Mn oxidation state, and the absorption peak of Mn(III)–O and Mn(IV)–O bonds has blue shift because of the doped Al. $LiAl_{0.05}Mn_{1.95}O_4$ powders (UASG) have the uniform, nearly cubic structure and octahedral morphology with narrow size distribution which is less than 1 μm. $LiAl_{0.05}Mn_{1.95}O_4$ (UASG) has a good reversibility and its structure is very advantageous for the transportation of lithium ions. The initial capacities of $LiMn_2O_4$ (sol–gel), $LiAl_{0.05}Mn_{1.95}O_4$ (sol–gel), and $LiAl_{0.05}Mn_{1.95}O_4$ (UASG) and capacity retention after 50 cycles at *C*/3 discharge rate are 130.9 mAh g^{-1}, 126.2 mAh g^{-1}, 127.9 mAh g^{-1} and 86.86%, 91.68%, 94.29%, respectively. The initial capacities of $LiMn_2O_4$ (sol–gel), $LiAl_{0.05}Mn_{1.95}O_4$ (sol–gel), and $LiAl_{0.05}Mn_{1.95}O_4$ (UASG) and capacity retention after 50 cycles at 1*C* discharge rate are 108.0 mAh g^{-1}, 105.0 mAh g^{-1}, 107.7 mAh g^{-1} and 79.22%, 83.46%, 86.57%, respectively, which reveals that the sample obtained via UASG method has the best electrochemical performance among three samples.

Acknowledgments

This work is partially supported by Harbin Institute of Technology. The author thanks Dr. Ying Wang of Institute of Chemistry Chinese Academy of Sciences for his helpful discussion on the experimental techniques.

References

[1] W.T. Jeong, J.H. Joo, K.S. Lee, J. Alloys Compd. 358 (2003) 294.
[2] R. Dziembaj, M. Molenda, J. Power Sources 119–121 (2003) 121.
[3] H. Gadjov, M. Gorova, V. Kotzeva, G. Avdeev, S. Uzunova, D. Kovacheva, J. Power Sources 134 (2004) 110.
[4] R.J. Gummow, A. de Knok, M.M. Thackeray, Solid State Ionics 69 (1994) 59.
[5] K. Matsuda, I. Taniguchi, J. Power Sources 132 (2004) 156.
[6] A. Yamada, J. Solid State Chem. 122 (1996) 160.
[7] Y.S. Lee, N. Kumada, M. Yoshio, J. Power Sources 96 (2001) 376.
[8] S.T. Myung, S. Komaba, N. Kumagai, J. Electrochem. Soc. 148 (2001) A482.
[9] B.L. He, S.J. Bao, Y.Y. Liang, W.J. Zhou, H.L. Li, J. Solid State Chem. 178 (2005) 897.
[10] S. Mukerjee, X.Q. Yang, X. Sun, S.J. Lee, J. McBreen, Y. Ein-Eli, Electrochim. Acta 20 (2004) 3373.
[11] Y.C. Sun, Z.X. Wang, X.J. Huang, L.Q. Chen, J. Power Sources 132 (2004) 161.
[12] H.Q. Li, L. Chen, Y.Y. Xia, Electrochem. Solid-State Lett. 8 (2005) A433.
[13] Q. Zhong, A. Bonakdarpour, M. Zhong, Y. Gao, J.R. Dahn, J. Electrochem. Soc. 144 (1997) 205.
[14] H.S. Fang, Z.X. Wang, X.H. Li, H.J. Guo, W.J. Peng, J. Power Sources 153 (2006) 174.
[15] T.F. Yi, D.L. Wang, K. Gao, X.G. Hu, J. Rare Earths 23 (Suppl.) (2005) 209.
[16] Y. Shao-Horn, R.L. Middaugh, Solid State Ionics 139 (2001) 13.
[17] K.M. Shaju, G.V. Subba Rao, B.V.R. Chowdari, Solid State Ionics 152–153 (2002) 69.
[18] G.G. Wang, J.M. Wang, W.Q. Mao, H.B. Shao, J.Q. Zhang, C.N. Cao, J. Solid State Electrochem. 9 (2005) 524.
[19] B. Ammundsen, G.R. Burns, M.S. Islam, H. Kanoh, J. Roziere, J. Phys. Chem. B 103 (1999) 5175.
[20] W. Huang, R. Frech, Solid State Ionics 86–88 (1996) 395.
[21] G.J. Exarhos, W.M. Risen Jr., Solid State Commun. 11 (1972) 755.
[22] J. Himmrich, H.D. Lutz, Solid State Commun. 79 (1991) 447.
[23] Y.-J. Kang, J.-H. Kim, Y.-K. Sun, J. Power Sources 146 (2005) 237.
[24] C.H. Lu, S.W. Lin, J. Power Sources 97–98 (2001) 458.
[25] Y.Y. Xia, H. Takeshige, H. Noguchi, M. Yoshio, J. Power Sources 56 (1995) 61.
[26] E.B. Flint, K.S. Suslick, Science 253 (1991) 1397.
[27] K.S. Suslick, G.J. Price, Annu. Rev. Mater. Sci. 29 (1999) 295.